Alexander F. Vakakis
Editor

International Centre
for Mechanical Sciences

Advanced Nonlinear Strategies for Vibration Mitigation and System Identification

CISM Courses and Lectures, vol. 518

SpringerWienNewYork

SpringerWienNewYork

CISM COURSES AND LECTURES

The series presents lecture notes, monographs, edited works and proceedings in the field of Mechanics, Engineering, Computer Science and Applied Mathematics.
Purpose of the series is to make known in the international scientific and technical community results obtained in some of the activities organized by CISM, the International Centre for Mechanical Sciences.

INTERNATIONAL CENTRE FOR MECHANICAL SCIENCES

COURSES AND LECTURES - No. 518

ADVANCED NONLINEAR STRATEGIES FOR VIBRATION MITIGATION AND SYSTEM IDENTIFICATION

EDITED BY

ALEXANDER F. VAKAKIS
UNIVERSITY OF ILLINOIS AT URBANA-CHAMPAIGN,
URBANA, ILLINOIS, USA

SpringerWienNewYork

This volume contains 156 illustrations

Printed in Italy
SPIN 80012994

All contributions have been typeset by the authors.

ISBN 978-3-7091-0204-6 SpringerWienNewYork

PREFACE

This book contains lecture material from CISM course No. 329 on 'Advanced Nonlinear Strategies for Vibration Mitigation and System Identification,' delivered in June 16-20, 2008 in Udine. The course addressed advanced nonlinear topics in the general areas of vibration mitigation and system identification, including topics such as, methods of analysis of strongly nonlinear dynamical systems; techniques and methodologies for interpreting complex, multi-frequency transitions in damped nonlinear responses; new approaches for passive vibration mitigation based on nonlinear targeted energy transfer (TET) and the associated concept of nonlinear energy sink (NES); and an overview and assessment of current nonlinear system identification techniques. In the general spirit of the course, effective nonlinear vibration and shock mitigation is closely tied to reliable nonlinear system identification of the underlying dynamics, so the two main topics of the course were regarded as closely interrelated. The contributions in this volume are structured as follows. First, a passive mitigation strategy for structures subjected to seismic loads is discussed, employing the concepts of nonlinear TET and NES (L.A. Bergman). This is followed by a discussion on the implementation of TET to problems of vibration mitigation of systems under steady state harmonic excitation, together with an exposition of nonlinear absorbers designed to act as NESs (O.V. Gendelman). There follows an overview and assessment of current nonlinear system identification techniques, structural model updating, and a discussion of the concept of nonlinear normal mode and its application to system identification (G. Kerschen). In the next contribution, analytical methods for studying resonant energy exchanges and TET in systems of coupled oscillators are discussed, including the new concept of the Limiting Phase Trajectory which holds promise as a powerful analytical tool for analyzing strongly nonlinear TET-related applications (L.I. Manevtich). A section related to issues on advanced signal processing and numerical computation follows, highlighting certain practical issues that need to be addressed when analyzing nonlinear experimental measurements (D.M. McFarland). Finally, an overview of the concepts of passive nonlinear TET and NES is provided, and some applications to problems of shock isolation are discussed (A.F. Vakakis).

We would like to thank the course participants for their valuable contributions in the form of discussions, questions and other feedback during the entire duration of the course, the CISM personnel for supporting so effectively the lecturers during their stay in Udine, and the editorial staff at Springer Verlag for helping with the preparation and publication of the final draft of the book. Of course, any errors that remain in the book are the responsibility of the authors.

Alexander F. Vakakis Urbana, 2009

CONTENTS

Mitigation Strategies for Systems Subjected to Vibratory, Shock and Seismic Loads

Lawrence A. Bergman*

* Department of Aerospace Engineering
University of Illinois at Urbana-Champaign
Urbana, Illinois, USA

Abstract. Worldwide, society has made a tremendous investment in constructed infrastructure, such as buildings and bridges. While the fraction of infrastructure vulnerable to large-scale earthquakes tends to be localized by geography (e.g., the Pacific Rim), there is ample evidence for widespread vulnerability. This strongly suggests the need to develop effective strategies to protect not only new construction but also existing structures likely to be subjected to damaging earthquakes. While various passive, semi-active and active methods for mitigating the effects of earthquakes have been designed for and in some cases applied to large scale structures, none has been shown to be simple, inexpensive, and widely applicable. We now examine the application of TET to the seismic protection of frame structures, in response to this need for a fully passive isolation strategy, lightweight and inexpensive but capable of high performance over a wide range of earthquakes of different properties.

1 Introduction

We now examine the application of TET to the seismic protection of frame structures. Infrastructure represents society's greatest investment. While the fraction of infrastructure vulnerable to large-scale earthquakes tends to be localized by geography (e.g., the Pacific Rim), recent devastating seismic activity in central Italy demonstrates the likelihood of widespread vulnerability. Thus, there is a need to develop effective strategies to protect not only new construction but also existing structures likely to be subjected to earthquakes.

Various passive methods for mitigating the effects of earthquakes have been applied to large scale structures, including auxiliary dampers, base isolation systems, tuned mass dampers, as well as active, semi-active and

hybrid systems. Detailed descriptions of each of these and a comparison of their performance are beyond the scope of this document. Rather, the interested reader should refer to several excellent monographs, including Soong and Constantino (1994); Soong (1990); Skinner et al. (1993); Chu et al. (2005), and recent review articles Housner et al. (1997); Spencer and Sain (1997); Soong and Spencer (2002); Spencer and Nagarajaiah (2003), as well as references therein for details. It seems clear, given the recent extensive body of literature and burgeoning number of isolated structures [1], that need exists for a fully passive isolation strategy, lightweight and inexpensive but capable of high performance over an extensive range of earthquakes of different properties.

We will demonstrate through a case study that it is possible to design and implement one or more NESs in a primary linear system with multiple degrees of freedom that will passively absorb and dissipate seismic energy drawn from the primary system as well as advantageously redistribute seismic energy within the modes of the primary system, thus enhancing its reliability and enabling performance under widely varying seismic conditions.

We will first introduce evaluation procedures for the protective system, including the choice of historic earthquakes and system performance criteria to be employed in the study. Then we will examine the seismic protection of a model three-story, single-bay, two-dimensional steel frame structure using, first, a single VI NES at the top floor and, second, a VI NES at the first floor and a smooth NES at the top floor. The design and optimization of each protective system configuration are discussed, and its performance is assessed both computationally and experimentally. This will be followed by a brief evaluation of protective system performance and some insights regarding possible full-scale implementation of the TET concept for seismic protection of civil infrastructural systems.

2 Evaluation Criteria

2.1 Description

The efficacy of TET for reduction of the seismic response of a primary structure depends on the ability of one or more attached NESs to passively

[1] According to Spencer and Nagarajaiah (2003), by 2003, more than 40 buildings and 10 bridges were constructed with integral active or hybrid seismic isolation systems. This does not include statistics for passive base isolation systems employing laminated rubber bearings, which for low-rise buildings have become ubiquitous in seismically-active regions.

absorb and dissipate a significant portion of the seismic energy at a sufficiently fast time scale. This ensures that the response of the primary structure is significantly reduced during the crucial initial few cycles of the strong motion. Thus, we will first develop an optimization procedure for choosing the parameters of the protective system so that its action is compatible with our design objectives, and then apply this procedure to study a scaled three degree of freedom steel frame, with NESs employed, subject to historic earthquakes. Details of NES design can be found in Georgiades (2006), Karayannis et al. (2008) and Lee et al. (2009).

2.2 Simulation and Optimization

System design and evaluation required an extensive series of simulations, employing Matlab® as the computational engine. The response of each system, including one or more NESs, was determined for four historic earthquakes as the excitation source. These included:

- El Centro, N-S component — May 18, 1940;
- Hachinohe, N-S component — May 16, 1968;
- Kobe, N-S component — January 17, 1995; and
- Northridge, N-S component — January 16, 1994.

As discussed in significant detail in Nucera (2005) and Nucera et al. (2007), these four were chosen as representative of two distinct classes of earthquakes. The first, containing the El Centro and Hachinohe records, are characterized by longer effective ground motion duration and smaller peak ground acceleration and velocity, while the second, containing Kobe and Northridge, exhibit shorter duration but larger peak ground acceleration and velocity. As noted in the references, Kobe has the highest energy content and destructive capacity of the four records.

The design space for the system optimization encompasses all NES parameters. The eight evaluation criteria, J_i, $i = 1, \ldots, 8$, employed to assign quantitative measures of performance to the computed seismic response of the system, are those introduced by Spencer et al. (1998b,c) in the context of a moderated benchmark control problem for a seismically excited structure.

$$J_1 = \max_{\text{earthquakes}} \left\{ \frac{\max\limits_{\substack{t \\ i \in \eta}} |u_i(t)|}{u^{\max}} \right\} \tag{1}$$

The first criterion (1) is a non-dimensional measure of the displacement relative to ground motion. Here, η represents the set of computed relative displacements, and $u^{\max}$ is maximum relative displacement for the uncon-

trolled (no NES) linear structure.

$$J_2 = \max_{\text{earthquakes}} \left\{ \frac{\max\limits_{i,j} \dfrac{|d_i(t)|}{h_i}}{d_n^{\max}} \right\} \tag{2}$$

The second criterion (2) is a normalized interstory drift ratio, where $d_i(t) = u_i(t) - u_{i-1}(t)$ is the time history of the ith interstory drift, h_i is the ith interstory height, and $d_n^{\max}$ is the maximum interstory drift for the uncontrolled structure.

$$J_3 = \max_{\text{earthquakes}} \left\{ \frac{\max\limits_{\substack{t \\ i\in\eta}} |\ddot{u}_{ai}(t)|}{\ddot{u}_a^{\max}} \right\} \tag{3}$$

The third criterion (3) is a normalized maximum absolute acceleration. Here, $\ddot{u}_{ai}(t)$ is the time history of absolute acceleration for the ith degree of freedom, and $\ddot{u}_a^{\max}$ is the maximum acceleration over all degrees of freedom for the uncontrolled structure.

$$J_4 = \max_{\text{earthquakes}} \left\{ \frac{\max\limits_{t} \sum\limits_{i\in\eta} m_i \ddot{u}_{ai}(t)}{F_b^{\max}} \right\} \tag{4}$$

The fourth criterion (4) is a normalized inertial force ratio, where $F_b^{\max}$ is the maximum base shear force for the uncontrolled structure.

$$J_5 = \max_{\text{earthquakes}} \left\{ \frac{\max\limits_{i\in\eta} \|u_i(t)\|}{\|u^{\max}\|} \right\} \tag{5}$$

The fifth criterion (5) is the L_2-normed measure of structural response. Here, $\|u_i(t)\| = \left[\int_0^t u_i^2(t)\,\mathrm{d}t\right]^{1/2}$, t_f is a sufficiently large time permitting the response of the structure to attenuate to less than 0.1% of its maximum value, and $\|u^{\max}\| = \max_{i\in\eta} \|u_i(t)\|$ is the maximum normed uncontrolled displacement.

$$J_6 = \max_{\text{earthquakes}} \left\{ \frac{\max\limits_{t,i} \dfrac{\|d_i(t)\|}{h_i}}{\|d_n^{\max}\|} \right\} \tag{6}$$

The sixth criterion (6) is a normed interstory drift ratio, where $\|d_n^{\max}\|$ is the maximum normed interstory drift for the uncontrolled structure.

$$J_7 = \max_{\text{earthquakes}} \left\{ \frac{\max_{i\in\eta} \|\ddot{u}_{ai}(t)\|}{\|\ddot{u}_a^{\max}\|} \right\} \tag{7}$$

The seventh criterion (7) is the normed absolute acceleration ratio, where $\|\ddot{u}_a^{\max}\|$ is the maximum normed absolute acceleration of the uncontrolled structure.

$$J_8 = \max_{\text{earthquakes}} \left\{ \frac{\left\| \sum_{i\in\eta} m_i \ddot{u}_{a\eta i}(t) \right\|}{\|F_b^{\max}\|} \right\} \tag{8}$$

The final criterion (8) is a normed inertial force ratio, where $\|F_b^{\max}\|$ is the maximum normed base shear force for the uncontrolled structure. We note here that all of the criteria are applied over the array of four historic earthquakes.

The method we employed to optimize the NES parameters is *differential evolution* (Storn and K., 1997; G., 2002), a global evolutionary optimization procedure. While each of the aforementioned criteria was evaluated over the array of four historic earthquakes, sufficient additional computations were completed to facilitate the determination of an optimal solution corresponding to each historic earthquake. Following Nucera (2005), a series of Pareto optimizations was performed utilizing the objective function

$$OF = J_1 + J_2 + J_3 + J_6. \tag{9}$$

3 Scaled Three-Story Steel Frame Structure with NESs

In this Section we examine the application of TET to a scaled three-story frame structure, subjected to the four historic earthquakes introduced in the previous section. The structure was designed and built in the Linear and Nonlinear Dynamics and Vibrations Laboratory (LNDVL) at the University of Illinois at Urbana-Champaign. The problem was motivated by a recent series of benchmarks designed to challenge the structural control community (Spencer et al., 1998b,c,a; Ohtori et al., 2004), though we were unable to duplicate and test any of those structures in our laboratory due to

physical limitations in our shake table capability. The design and characterization of our structure were accomplished through a combination of finite element computations and experimental modal analysis. Once the model was completely defined, several protective system configurations employing NESs were designed, optimized, and verified experimentally. One configuration in particular was shown to provide a significant level of protection for all four earthquakes examined, remarkable in view of the fully passive design. A description of the analysis and design processes as well as the mechanics of our protective systems follow.

3.1 Characterization of the Three-Story Linear Frame Structure

Following Nucera (2005); Nucera et al. (2009, 2008), the structure (i.e., the linear primary system), shown in Figure 1, is a three-story, one-bay frame with spring steel columns and polypropylene floor slabs, approximately 60 cm tall, 20 cm wide and 10 cm deep. The floors slabs are bolted directly to the columns, through small aluminum plates to increase rigidity, using 4 cap screws per connection. The foundation, also polypropylene, was bolted directly to a mechanical shake table (Figure 2) through which the historic earthquake time histories were applied. The floor slabs were sufficiently thick in dimension to ensure adequate rigidity against bending; thus, the frame was designed to respond as a shear beam, with each column modeled as a clamped-clamped Euler-Bernoulli beam with lateral stiffness $k = 12EI/h^3$. Here, E is Young's modulus for spring steel, I is the area moment of inertia of the column about its bending axis, and h is the effective column length of a story. The resulting floor masses are assumed to be equal at 1.127 kg, and the column stiffnesses, also assumed equal, are rounded off to 5000 N/m.

The frame is governed by the equation of motion

$$M\ddot{u} + C\dot{u} + Ku = -MI_0\ddot{u}_g \tag{10}$$

where the mass and stiffness matrices, displacement vector relative to ground motion, and input distribution vector are given, respectively, by

$$M = \begin{bmatrix} m_1 & 0 & 0 \\ 0 & m_2 & 0 \\ 0 & 0 & m_3 \end{bmatrix}, \quad K = \begin{bmatrix} 2k & -k & 0 \\ -k & 2k & -k \\ 0 & -k & k \end{bmatrix},$$

$$u(t) = \begin{Bmatrix} u_1 \\ u_2 \\ u_3 \end{Bmatrix}, \quad I_0 = \begin{Bmatrix} 1 \\ 1 \\ 1 \end{Bmatrix}$$

and $\ddot{u}_g$ is the ground acceleration. We considered the case where the system is proportionally damped and determined the modal damping factors

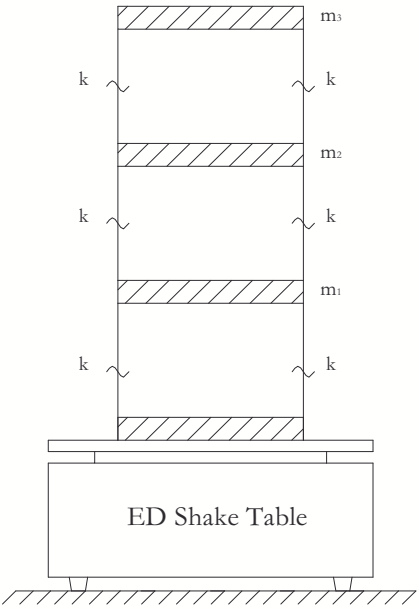

Figure 1. Sketch of the three-story, one-bay steel and polypropylene frame structure shown mounted to an electromechanical shake table.

from an experimental modal analysis of the structure. Here, the mechanical shaker was locked down, and an impact hammer with an integral piezoelectric force transducer was employed to provide the necessary impulsive excitation at each story. Responses were measured using a piezoelectric accelerometer at each story, as shown in Figure 3. All transducers used were manufactured by PCB Piezotronics, Inc. Data was subsequently acquired through a SigLab signal analysis system, and both impulse responses and complex frequency responses were saved for further analysis.

The experimental modal analysis was performed in the time domain using the Ibrahim Time Domain (ITD) method (Ibrahim and Pappa, 1982; G., 2002), and frequency domain using the Rational Fraction Polynomial (RFP) method, the latter implemented in the Diamond software package made available by the Los Alamos National Laboratory (Doebling et al., 1997). The average of the two methods gave natural frequencies of 4.6, 12.8, and 18.3 Hz, compared with computational values of 4.7, 13.2, and 19.1 Hz, resulting in a consistently high error ranging from two to four percent, which we attribute primarily to unmodeled compliance in the table/support

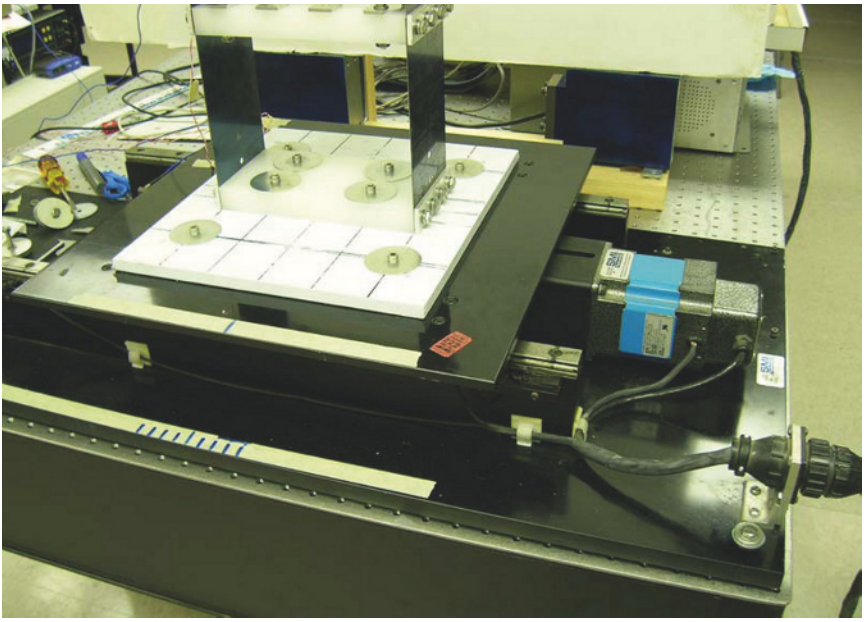

Figure 2. Detail showing mounting of the steel frame to the locked-down shake table.

assembly. However, the close agreement in natural frequency makes the damping estimates, again the average of ITD and RFP results, credible. The modal damping factors were found to be 0.00275, 0.00313, and 0.00236 for modes one through three, respectively. The modal damping matrix $\hat{C}$ was then determined, from which the viscous damping matrix was computed. This completed the determination of the linear portion of the simulation model.

3.2 Simulation and Optimization of the Frame-Single VI NES System

A VI NES was attached to the top (third) floor of the primary system in order to utilize the large building displacements at that height to maximize its authority, as shown in the schematic of Figure 4. The equations of motion reflect the NES degree of freedom added to the equations of the 3

(a)

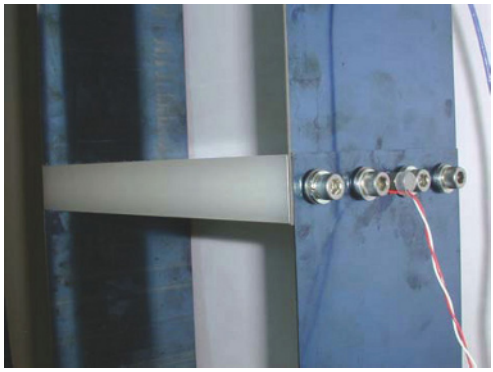

(b)

Figure 3. The three-story uncontrolled frame undergoing modal testing using an impact hammer to determine its eigenspectrum and modal damping factors: (a) excitation using a modal hammer, (b) typical accelerometer installation.

degree of freedom primary system, giving

$$M = \begin{bmatrix} m_1 & 0 & 0 & 0 \\ 0 & m_2 & 0 & 0 \\ 0 & 0 & m_3 & 0 \\ 0 & 0 & 0 & m_{\mathrm{NES}} \end{bmatrix}, \quad C = \begin{bmatrix} \lambda_1+\lambda_2 & -\lambda_2 & 0 & 0 \\ -\lambda_2 & \lambda_2+\lambda_3 & -\lambda_3 & 0 \\ 0 & -\lambda_3 & \lambda_3 & 0 \\ 0 & 0 & 0 & 0 \end{bmatrix},$$

$$K = \begin{bmatrix} 2k & -k & 0 & 0 \\ -k & 2k & -k & 0 \\ 0 & -k & k+k_{\mathrm{NES}} & -k_{\mathrm{NES}} \\ 0 & 0 & -k_{\mathrm{NES}} & k_{\mathrm{NES}} \end{bmatrix}, \quad I_0 = \begin{Bmatrix} 1 \\ 1 \\ 1 \\ 1 \end{Bmatrix}, \quad u(t) = \begin{Bmatrix} u_1 \\ u_2 \\ u_3 \\ u_{\mathrm{NES}} \end{Bmatrix}$$

where k_{NES} is small compared with k.

Adding the VI NES makes the combined system piecewise linear; i.e., between any two consecutive impacts of m_{NES} the system is linear. Hence, the numerical integration of the equations of motion requires the solution of a sequence of linear initial value problems, each of which is bounded by successive vibro-impacts of the NES. The precise computation of the times at which vibro-impacts occur is necessary for accurate simulation of the transient dynamics of the system, as they determine the temporal boundaries of the linear computations. When a vibro-impact occurs, the computation is halted, the initial conditions are modified to account for the state of the system post-impact, and the computation then resumes. The relation for the velocities of the affected masses before and after impact is

$$v_3' - v_{\mathrm{NES}}' = rc(v_{\mathrm{NES}} - v_3), \tag{11}$$

where rc is the coefficient of restitution, and as before, while energy is not conserved through the inelastic impact, momentum is conserved, leading to

$$m_3 v_3 + m_{\mathrm{NES}} v_{\mathrm{NES}} = m_3 v_3' + m_{\mathrm{NES}} v_{\mathrm{NES}}'. \tag{12}$$

The system of equations was reduced to state-space form and integrated using function ODE45 in Matlab®, taking advantage of its adaptive time-stepping to achieve the required accuracy in the vicinity of each impact.

The optimization parameters were those of the VI NES (i.e. m_{NES}, k_{NES}, e, and rc), and the evaluation criteria, objective function, and procedure were those discussed previously. The optimization was performed over the array of four historic earthquakes, with an optimal solution determined for each particular earthquake. Both the Northridge and Kobe results will be discussed further as they represent the more severe case within each earthquake class.

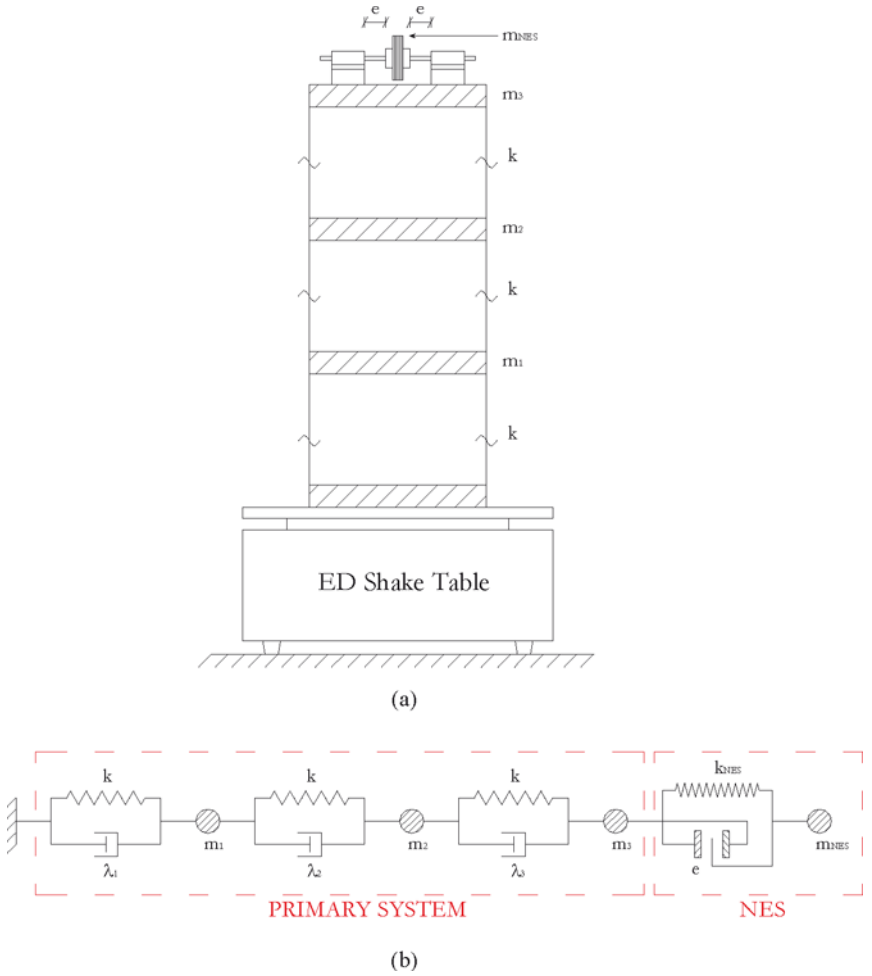

Figure 4. Sketch (a) and schematic (b) of the three-story, one-bay steel and polypropylene frame structure with a single VI NES attached to the third floor.

4 Optimal NES Design for the Northridge Earthquake

Prior to initiating the study, examination of the Fourier spectrum of the Northridge acceleration record revealed that a mismatch existed between the frequency bandwidth of maximum energy content and the eigenspectrum of the three story structure. In order to place the maximum energy of the earthquake in a frequency band consistent with the eigenspectrum, the duration of the earthquake was scaled by a factor of one half to twenty five seconds from its original fifty, thus doubling its effective bandwidth and ensuring that the computed response represents the most severe condition. The acceleration amplitude, however, was left unscaled.

It was observed throughout the ensuing simulations that during the strong motion portion of the earthquake, the VI NES was able to respond quickly, resulting in vibro-impacts that dissipate a significant portion of the input energy. This is a signal advantage of the VI NES over the smooth NES, which acts more slowly and is unable to affect structural response during the first few critical cycles of strong motion. The optimal VI NES parameters for the Northridge record were determined to be: m_{NES} equal to 4% of the total mass of the primary system; $k_{\mathrm{NES}} = 0.005k$; $rc = 0.40$; and $e = 0.02\,\mathrm{m}$. The natural frequencies of the system including the VI NES were computed to be 2.2, 4.6, 12.8, and 18.3 Hz, reflecting the addition of the new, low-frequency mode due to the weakly coupled NES mass at the top floor.

Figure 5 provides a comparison between the controlled and uncontrolled (no NES) relative displacements with respect to ground of each floor of the frame, while Figure 6 compares the absolute displacement of the third floor with that of the NES and gives the phase plot of the response of the NES relative to the third floor as well as the instantaneous total energy dissipated at each vibro-impact and the vibro-impact time history. The last of these provides a measure of the severity of vibro-impacts, indicating whether there is sufficient interaction between the primary system and NES.

Wavelet spectra of the relative displacements between the first floor and ground, the second and first floors, and the third and second floors are shown in Figure 7, clearly depicting the scattering of energy to all structural modes due to vibro-impacts of the NES. We note that the uncontrolled structure responds primarily at its first mode of 4.6 Hz, which leads to large relative displacements. In the presence of the NES, however, seismic energy is spread to as many as four linear modes, with the spreading becoming more pronounced at the higher floors. This is a two-fold advantage from the mitigation standpoint and explains the reduced levels of structural response

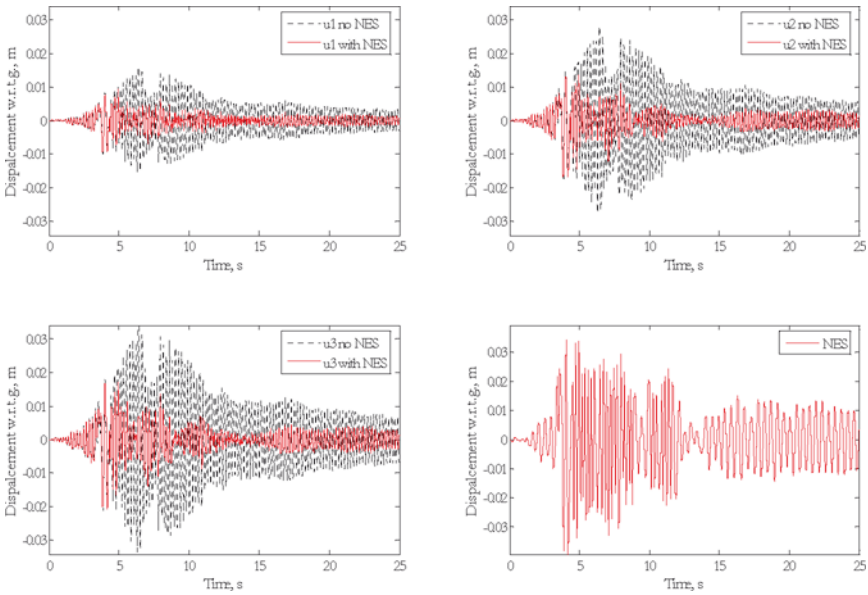

Figure 5. Comparison of uncontrolled and controlled floor displacements relative to ground and the VI NES displacement relative to ground for the system optimized for and subjected to the Northridge earthquake.

observed with the NES in place. First, due to the vibro-impacts, seismic energy is transferred from the low frequency, high amplitude first structural mode to the lower amplitude, higher frequency structural modes where it is more readily dissipated by internal damping effects; second, energy "leaking" to the lowest mode at 2.2 Hz results in even greater mitigation as that mode is localized to the NES.

The performance of the optimized system can be visualized through the evaluation criteria

$$(J_1, J_2, \ldots, J_8) = (0.61, 0.59, 0.80, 0.58, 0.37, 0.39, 0.57, 0.39).$$

Thus, a 39% reduction in maximum displacement (see J_1) and a 41% reduction in maximum interstory drift (see J_2) are realized compared to the uncontrolled system, with the normed criteria reduced even more.

Examination of the controlled responses of Figures 5 and 6 reveals three distinct phases. During the first three seconds, the relative motion between the NES and third floor is less than the clearance so that no vibro-impacts

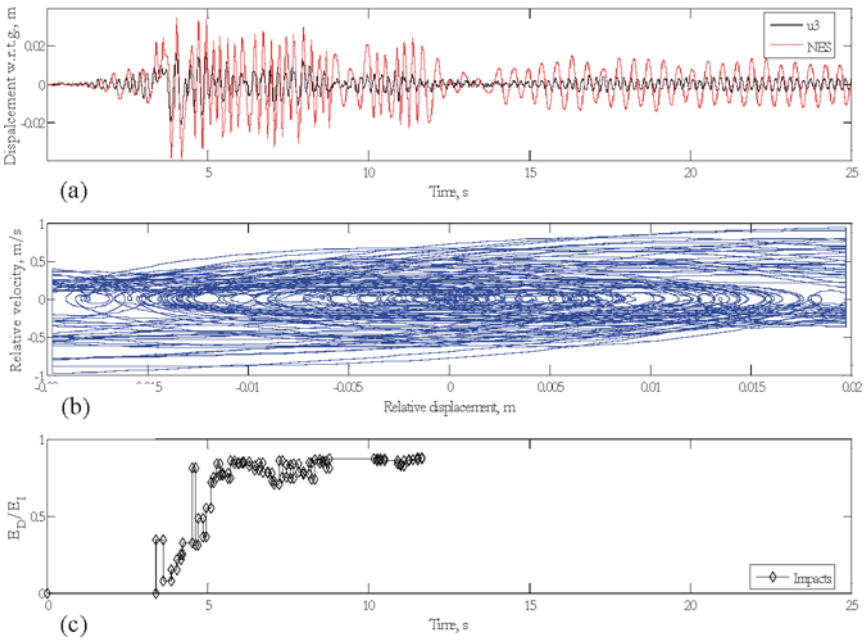

Figure 6. Performance of the VI NES optimized for and subjected to the Northridge earthquake: (a) comparison between absolute displacements of the third floor and the NES; (b) phase plot of relative velocity vs. relative displacement between the third floor and NES; and (c) energy dissipation by the VI NES showing the portion of instantaneous seismic energy dissipated during each vibro-impact.

occur and the system is linear. In the second phase, from three to eight and a half seconds, strong vibro-impacts occur due to a $1:1$ transient resonance capture between the first structural mode and the VI NES, resulting in dissipation of approximately eighty-seven percent of the input seismic energy. The final phase occurs after escape from resonance capture; however, a series of vibro-impacts occurs between ten and twelve seconds, though efficient energy dissipation is not achieved since the earthquake has released nearly all of its energy by eight seconds. This confirms that the VI NES is effective from the first cycle of response and is able to dissipate seismic energy at a sufficiently fast time scale to mitigate large responses at early time typical of near-field events. This fundamental mechanism, in conjunction with the spreading phenomenon already discussed, provides an effective mitigation

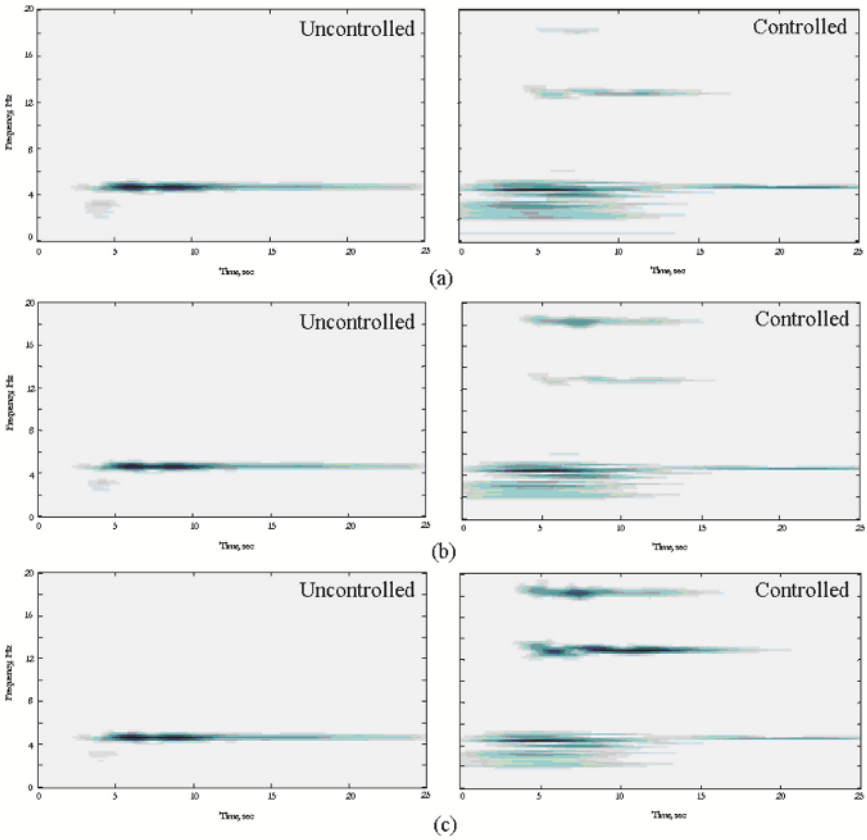

Figure 7. Comparisons between the wavelet spectra of controlled and uncontrolled relative displacements for a primary system with Northridge-optimized VI NES attached to the third floor and Northridge seismic excitation: (a) $u_1(t) - u_g(t)$, (b) $u_2(t) - u_1(t)$, (c) $u_3(t) - u_2(t)$.

strategy for large scale structures.

5 Optimal NES Design for the Kobe Earthquake

Optimization of the VI NES system for the Kobe earthquake followed that of the Northridge earthquake, just discussed. Again, in order to tune the earthquake record to the eigenspectrum of the structure, the record was scaled to twenty five seconds from the original duration of fifty seconds, doubling its frequency bandwidth; acceleration amplitude was not scaled. The optimal VI NES parameters for the Kobe record were determined to be: m_{NES} equal to 4.5% of the total mass of the primary system; $k_{\mathrm{NES}} = 0.004k$; $rc = 0.40$; and $e = 0.018\,\mathrm{m}$. The natural frequencies of the system including the VI NES were computed to be 1.7, 4.6, 12.8, and 18.3 Hz, reflecting the addition of the new, low-frequency mode due to the weakly coupled NES mass at the top floor.

Figure 8 provides a comparison between the controlled and uncontrolled (no NES) relative displacements with respect to ground of each floor of the frame, while Figure 9 compares the absolute displacement of the third floor with that of the NES and gives the phase plot of the response of the NES relative to the third floor as well as the instantaneous total energy dissipated at each vibro-impact and the vibro-impact time history. The last of these provides a measure of the severity of vibro-impacts, indicating whether there is sufficient interaction between the primary system and NES.

Wavelet spectra of the relative displacements between the first floor and ground, the second and first floors, and the third and second floors are shown in Figure 10, again depicting the scattering of energy to all structural modes due to vibro-impacts of the NES. In the presence of the VI NES, seismic energy is spread to the linear modes as before, resulting in dissipation and reduction in response.

It would be desirable if a protective system designed and optimized specifically for a particular, severe historic earthquake acting on a known structure functioned in near-optimal fashion for a range of historic earthquakes. Thus, we examined the system resulting from the Kobe analysis in terms of its performance under the El Centro, Hachinohe and Northridge records. Both the El Centro and Hachinohe acceleration records were scaled in time to 50% of their original length, with the amplitude left unscaled. Comparisons of controlled and uncontrolled displacements relative to ground, and the NES displacement relative to ground, for the El Centro, Hachinohe and Northridge earthquake records are given in Figures 11, 12 and 13, respectively. That there is a dramatic reduction in response for all three systems is clear from the plots.

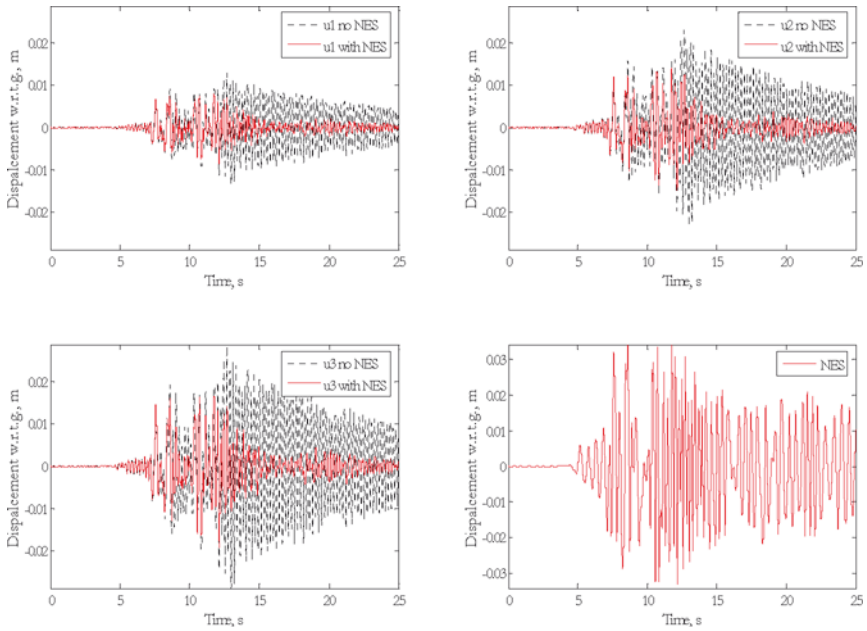

Figure 8. Comparison of uncontrolled and controlled floor displacements relative to ground and the VI NES displacement relative to ground for the system optimized for and subjected to the Kobe earthquake.

The eight evaluation criteria for the Kobe-designed system subjected to all four historic earthquake records are given in Table 2. Reductions in maximum displacement and maximum interstory drift were 36% and 38%, respectively, for Kobe, 36% and 36% for Northridge, 50% and 51% for El Centro, and 39% and 42% for Hachinohe. In all cases, reductions in the normed criteria were equally impressive.

This cursory study demonstrates that the VI NES can be an efficacious element of a control strategy for seismic protection of shear beam structures. We noted in the course of this study, however, that the VI NES functions most effectively during the strong motion segment of the earthquake, losing its ability to undergo vibro-impacts as the input energy decreases and, in the limit, reaching a no-impact condition where it becomes ineffective. This condition will be exacerbated for the case of earthquakes of low-to-moderate intensity, with seismic energy well below that of the design earthquake. Thus, we now consider a second, alternate design based upon the combined

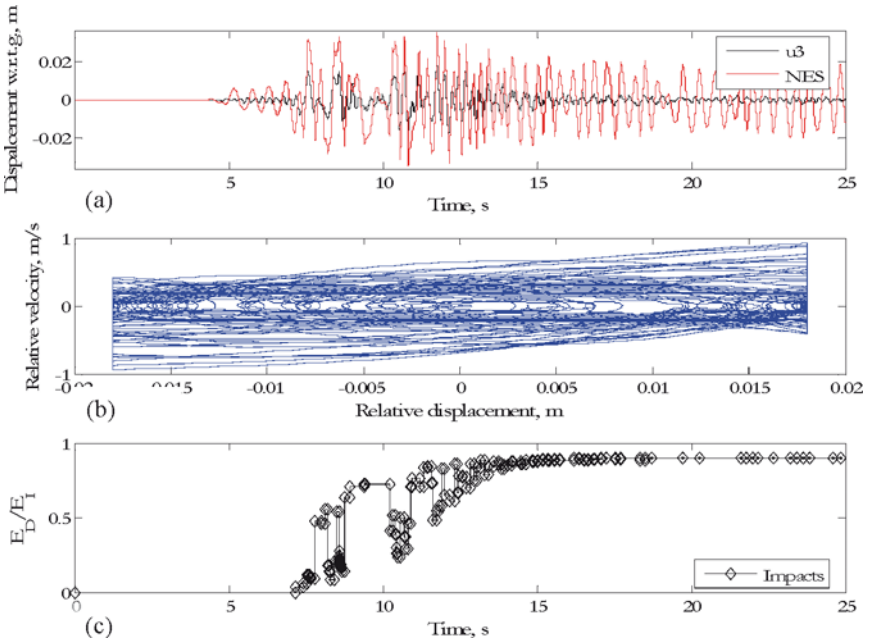

Figure 9. Performance of the VI NES optimized for and subjected to the Kobe earthquake: (a) comparison between absolute displacements of the third floor and the NES; (b) phase plot of relative velocity vs. relative displacement between the third floor and NES; and (c) energy dissipation by the VI NES showing the portion of instantaneous seismic energy dissipated during each vibro-impact.

utilization of a VI NES and a smooth NES, in order to extend the useful range of the TET strategy for seismic protection of structures.

5.1 Simulation and Optimization of the Frame-VI NES-Smooth NES System

We now attach a smooth NES incorporating an essentially nonlinear cubic spring to the top (third) floor of the primary structure and a VI NES to the first floor, as shown in Figure 14. The intent of this design is to combine a lightweight smooth NES design, which will perform adequately for moderate-to-severe earthquakes, and a relatively heavy VI NES for protection from severe, possibly near field, events. As the more massive VI NES is positioned lower in the structure, its effect upon the structural design will

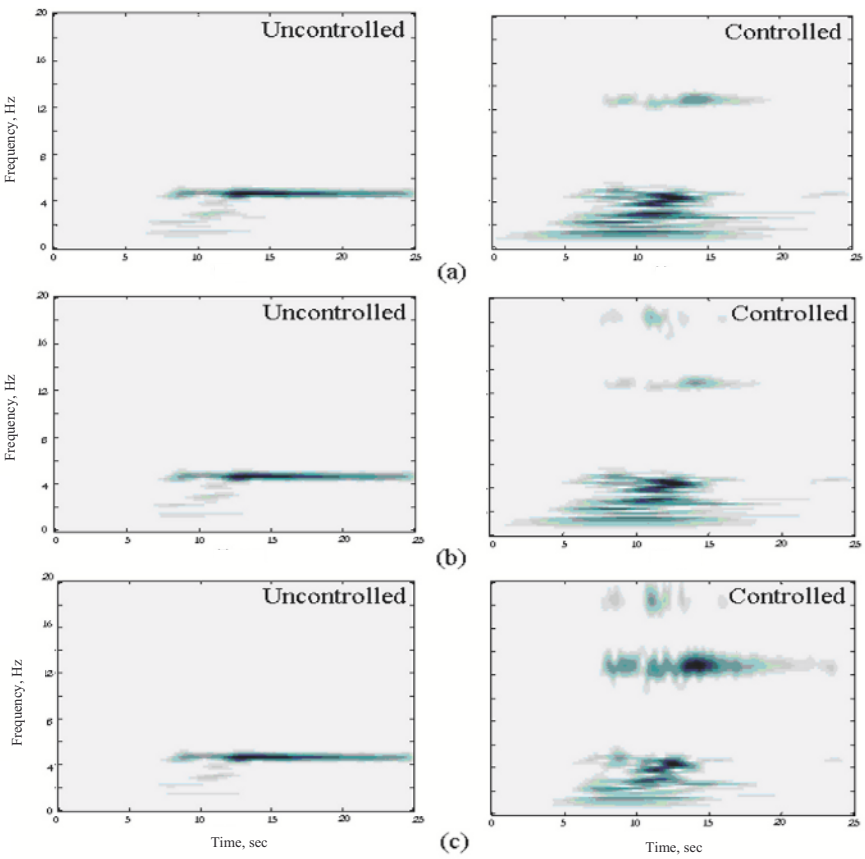

Figure 10. Comparisons between the wavelet spectra of controlled and uncontrolled relative displacements for a primary system with Kobe-optimized VI NES attached to the third floor, and Kobe seismic excitation: (a) $u_1(t) - u_g(t)$, (b) $u_2(t) - u_1(t)$, (c) $u_3(t) - u_2(t)$.

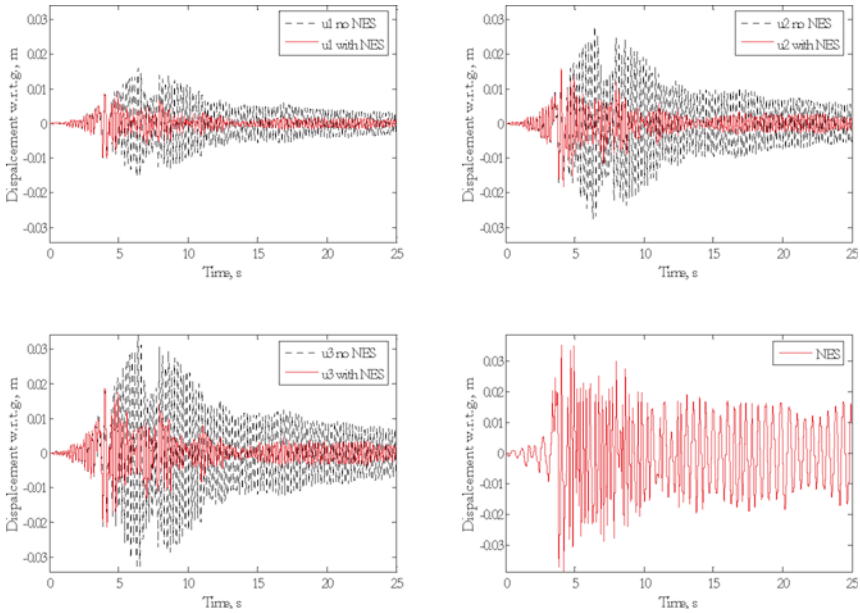

Figure 11. Uncontrolled and controlled displacements relative to ground when a Kobe-optimized VI NES is attached to the third floor of the frame, subjected to the Northridge excitation.

be minimized; the smooth NES at the top floor will continue to function even as the available seismic energy input becomes relatively small.

The equations of motion are now given by

$$M\ddot{u} + C\dot{u} + Ku = -MI_0\ddot{u}_g + f \tag{13}$$

where, following the previous section, the mass, damping and stiffness ma-

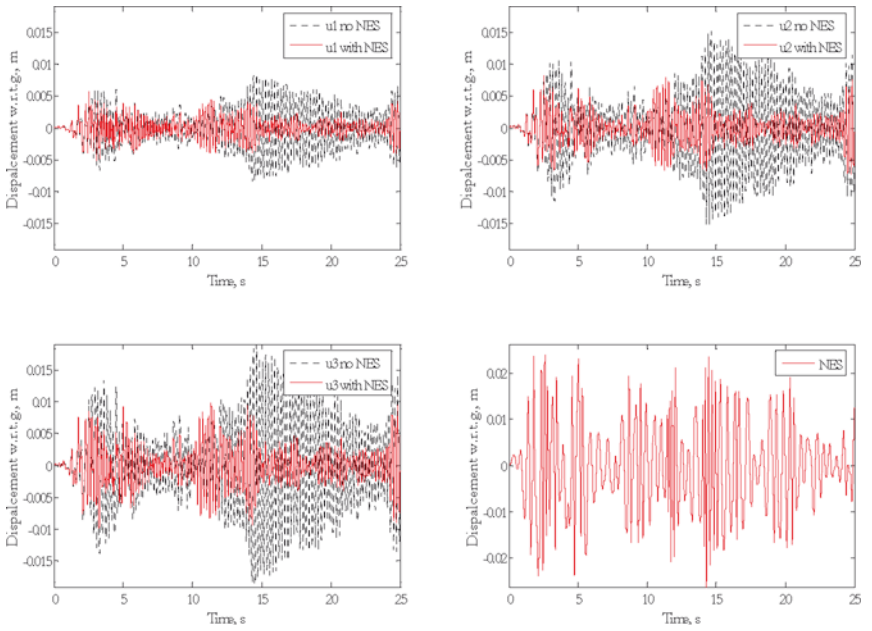

Figure 12. Uncontrolled and controlled displacements relative to ground when a Kobe-optimized VI NES is attached to the third floor of the frame, subjected to the El Centro excitation.

trices and displacement vector relative to ground are

$$M = \begin{bmatrix} m_1 & 0 & 0 & 0 & 0 \\ 0 & m_2 & 0 & 0 & 0 \\ 0 & 0 & m_3 & 0 & 0 \\ 0 & 0 & 0 & m_{\mathrm{NES}_1} & 0 \\ 0 & 0 & 0 & 0 & m_{\mathrm{NES}_2} \end{bmatrix},$$

$$C = \begin{bmatrix} \lambda_1 + \lambda_2 & -\lambda_2 & 0 & 0 & 0 \\ -\lambda_2 & \lambda_2 + \lambda_3 & -\lambda_3 & 0 & 0 \\ 0 & -\lambda_3 & \lambda_3 + \lambda_4 & 0 & -\lambda_4 \\ 0 & 0 & 0 & 0 & 0 \\ 0 & 0 & -\lambda_4 & 0 & \lambda_4 \end{bmatrix},$$

$$K = \begin{bmatrix} 2k + k_{\mathrm{NES}_1} & -k & 0 & -k_{\mathrm{NES}_1} & 0 \\ -k & 2k & -k & 0 & 0 \\ 0 & -k & k & 0 & 0 \\ -k_{\mathrm{NES}_1} & 0 & 0 & k_{\mathrm{NES}_1} & 0 \\ 0 & 0 & 0 & 0 & 0 \end{bmatrix}, \quad u(t) = \begin{Bmatrix} u_1 \\ u_2 \\ u_3 \\ u_{\mathrm{NES}_1} \\ u_{\mathrm{NES}_2} \end{Bmatrix}$$

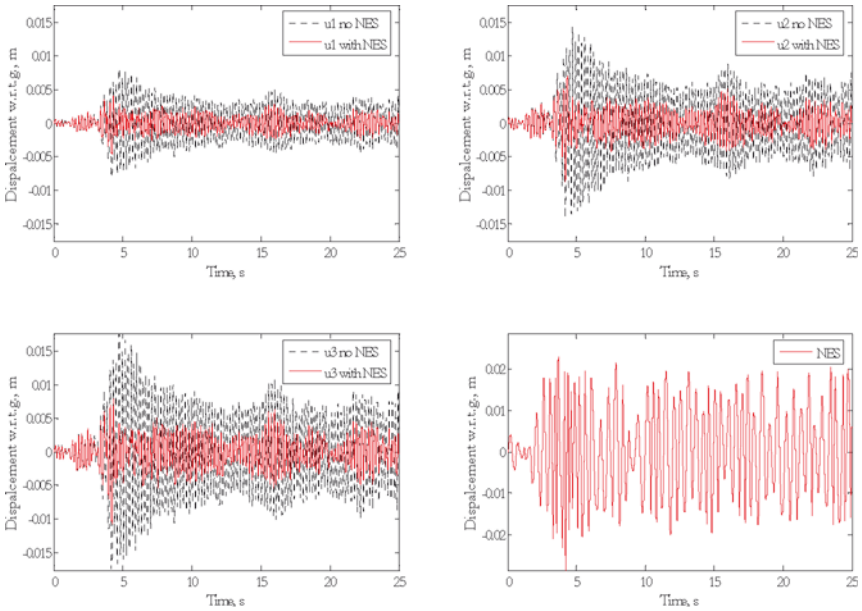

Figure 13. Uncontrolled and controlled displacements relative to ground when a Kobe-optimized VI NES is attached to the third floor of the frame, subjected to the Hachinohe excitation.

Table 1. Evaluation criteria for four historic earthquakes; linear frame with Kobe-designed single-VI NES at floor 3.

Earthquake	J_1	J_2	J_3	J_4	J_5	J_6	J_7	J_8
Kobe	0.64	0.62	0.98	0.62	0.42	0.45	0.61	0.45
Northridge	0.64	0.64	0.92	0.65	0.39	0.40	0.51	0.40
El Centro	0.50	0.69	1.00	0.69	0.38	0.43	0.78	0.43
Hachinohe	0.61	0.58	1.00	0.57	0.39	0.41	0.51	0.41

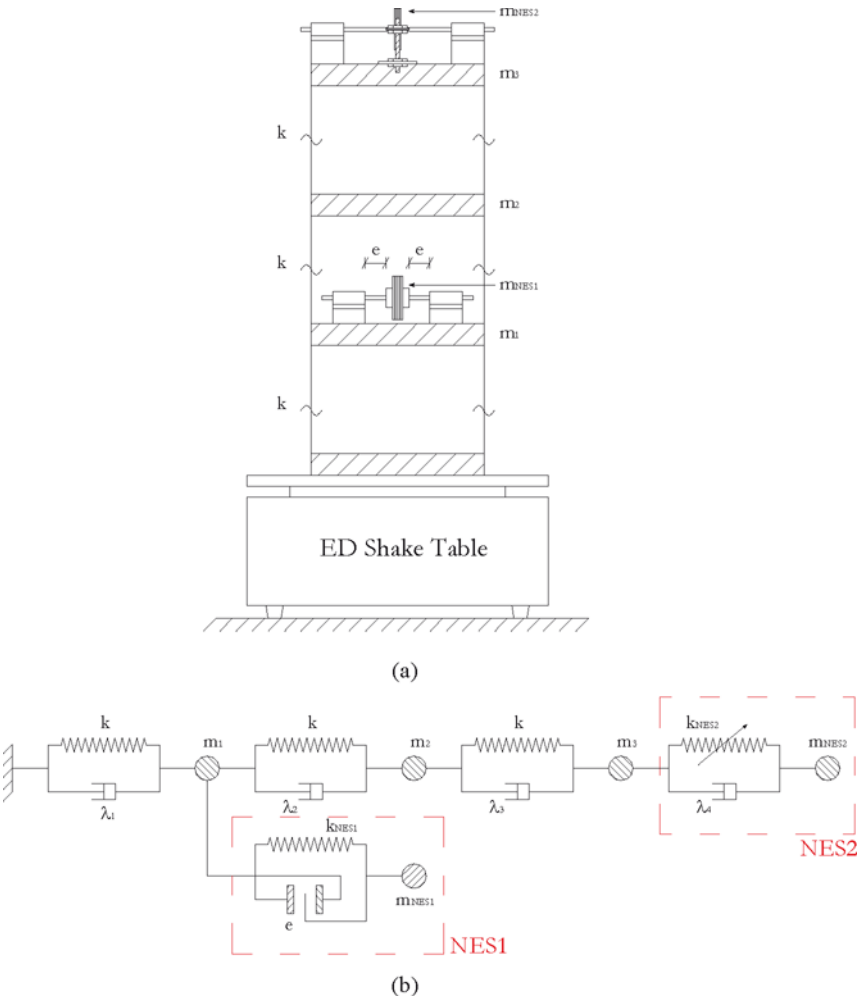

Figure 14. Sketch (a) and schematic (b) of the three-story, one-bay steel and polypropylene frame structure with a single-VI NES attached to the first floor and a smooth NES attached to the third floor.